Passivation Using Molecular Halides Increases Quantum Dot Solar Cell Performance

Xinzheng Lan, Oleksandr Voznyy, Amirreza Kiani, F. Pelayo García de Arquer, Abdullah Saud Abbas, Gi-Hwan Kim, Mengxia Liu, Zhenyu Yang, Grant Walters, Jixian Xu, Mingjian Yuan, Zhijun Ning, Fengjia Fan, Pongsakorn Kanjanaboos, Illan Kramer, David Zhitomirsky, Philip Lee, Alexander Perelgut, Sjoerd Hoogland, and Edward H. Sargent*

Colloidal quantum dot (CQD) solar cells have advanced significantly in performance over the past decade.[1–4] CQD solar cells offer several benefits over other thin-film technologies. The size-dependent bandgap of CQDs enables harnessing the infrared regions of the solar spectrum wavelengths not captured using most other photovoltaic (PV) materials. This property makes CQD solar cells good candidates for the back cell atop visible and NIR-bandgap PV materials (e.g., perovskite and silicon) and allows for the construction of tandem and multijunction architectures.[5–7] Additionally, multiple exciton generation, specific to CQDs, offers an avenue to reduce thermalization losses and increase the utilization of the solar fluence.[8,9] Recent progress in CQD solar cell power conversion efficiency (PCE) has been accompanied by improvements in device stability,[2,10,11] which further increases their promise.

Improved light absorption and charge collection are the two major requirements for increasing solar cell efficiency.[12,13] Photon management techniques, such as nanoscale plasmonic inclusions[14,15] and hierarchically structured electrodes,[3,16] have demonstrated enhanced light absorption in CQD solar cells. Significant improvements in charge extraction have been achieved as the device architecture progressed from Schottky-junction to depleted heterojunction,[17–19] bulk heterojunction,[20–24] and quantum junction devices.[2,11,25,26]

While notable advances in performance have been accomplished through the aforementioned efforts, further progress still relies on addressing the quality of the light-absorbing film itself.[27–31] In CQD solids, the large surface-to-volume ratio results in added opportunities for electronic defect formation. Increased recombination losses risk compromising the charge collection if not suitably addressed. Ligand-assisted surface passivation is a proven strategy to combat these losses. A range of short-chain-organic (e.g., mercaptopropionic acid, ethanedithiol, thiocyanate) and inorganic ligands (e.g., Cl⁻, Br⁻, I⁻) have been explored for this purpose.[19,32–36] These surface passivation schemes have been carried out based on solid-state ligand exchange processes driven by the difference in CQD-ligand binding strengths.[37] Ideally, the ligand exchange approach will preserve the passivation state existing prior to the exchange process (i.e., the passivation state of long-chain organic-ligand-capped CQDs). However, it is unlikely to repair any trap states already present in the as-synthesized CQDs. New passivation strategies, applied before the solid-state ligand exchange, could thus potentially further improve CQD characteristics.

Here we report a solution-based passivation scheme that features a redox reaction ($PbS + I_2 = PbI_2 + S$) occurring at the PbS CQDs surface in the presence of iodine molecules (I_2) dissolved in a nonpolar solvent. Solution treatment allows for increased control over halogen reactivity, helping to avoid overtreatment and improving overall passivation of CQDs in solution.[38,39] Better-passivated CQDs resulting from the optimized reactivity show a longer carrier diffusion length in film. Hence, we were able to fabricate photovoltaic devices with a thicker active region without compromising the charge collection. This optimization ultimately led to CQD solar cells with certified power conversion efficiency (PCE) of 9.9%. This is the highest certified PCE for CQD solar cells.

X-ray photoelectron spectroscopy (XPS) confirms the adsorption of iodine on the surface of PbS CQDs following I_2 treatment (**Figure 1**a). The amount of I_2 applied to the CQDs was systematically optimized in order to avoid overtreatment (see the Experimental Section). In developing the I_2-treatment process, we have found that the quantity of applied I_2 plays a crucial role. Under the optimized I_2 treatment conditions, the CQDs maintain good monodispersity (see Figure S1a, Supporting Information). Heavier than optimized I_2 treatment leads to several undesirable effects, such as stripping of an undesirably large number of ligands from the QD surface, causing QDs to fuse (see Figure S1b, Supporting Information).

Dr. X. Lan, Dr. O. Voznyy, A. Kiani,
Dr. F. P. García de Arquer, A. S. Abbas,
Dr. G.-H. Kim, M. Liu, Dr. Z. Yang, G. Walters,
J. Xu, Dr. M. Yuan, Dr. F. Fan, Dr. P. Kanjanaboos,[+]
Dr. I. Kramer, Dr. D. Zhitomirsky, P. Lee, A. Perelgut,
Dr. S. Hoogland, Prof. E. H. Sargent
Department of Electrical and Computer Engineering
University of Toronto
10 King's College Road, Toronto, Ontario M5S 3G4, Canada
E-mail: ted.sargent@utoronto.ca
Prof. Z. Ning
School of Physical Science and Technology
Shanghai Tech University
100 Haike Rd., Pudong New Area, Shanghai 201210, China
[+]Present address: Materials Science and Engineering, Faculty of Science, Mahidol University, 272 Rama 6 Rd., Ratchathewi District, Bangkok 10400, Thailand
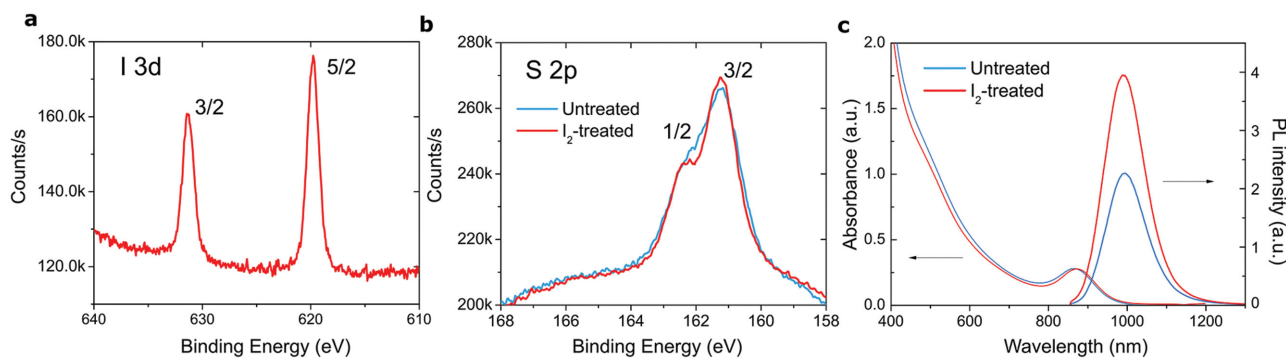
Figure 1. Characterization of I$_2$ passivation on PbS CQDs following the I$_2$ treatment. a) I 3d peak showcasing the successful incorporation of iodine into the dots. b) The S 2p XPS spectrum showing differences in local environment for sulfur in untreated and I$_2$ solution-treated CQDs. c) Absorption and photoluminescence spectra of untreated and I$_2$-treated PbS CQDs in the solution phase. No changes in monodispersity are observed. The increase of photoluminescence intensity after I$_2$ treatment is consistent with improved surface passivation.

It can contribute to excessive n-type doping due to changes in stoichiometry and lead to self-compensation via surface reconstruction and trap formation.[40,41] This overtreatment results in devices with poor efficiency due to decreased V_{oc} and fill factor (see Figure S2, Supporting Information). The optimal I:Pb ratio in XPS is found to be 5% which corresponds to ≈15–25% of available surface S sites.[27] The narrower XPS peaks for sulfur after I$_2$ treatment (Figure 1b) indicates a more homogeneous local environment for sulfur atoms. This may arise from the elimination of surface sulfur sites with reduced coordination by replacing them with iodine (Figure S3, Supporting Information), considering that the eliminated sites possessed a distinct XPS signature compared to fully coordinated S in the bulk of PbS.

The absorption spectra of the PbS CQDs before and after I$_2$ treatment (Figure 1c) show no appreciable change in the exciton peak position, suggesting that CQD size is not affected by the process. At the same time, photoluminescence spectra of the dots show that the the full-width-at-half-maximum is preserved, proving that ensemble monodispersity remained intact. The photoluminescence quantum yield (PLQY) of the dots with and without I$_2$ treatment are 19% and 15%, respectively, an indication of improved surface passivation.

We next sought to take advantage of the improved CQDs passivation by incorporating them into solar cells with an improved quantum-junction architecture (**Figure 2**a).[11,26] Tetrabutylammonium iodide (TBAI)-exchanged PbS CQD film (7–8 layers), serving as the n-type active region, was deposited on ZnO-nanoparticle-coated indium-doped tin oxide (ITO) glass substrates. This was followed by 2 layers of p-type CQD film prepared via ethanedithiol (EDT) exchange.[2] It should be noted that the bandgap of the CQDs used in this study was blue-shifted compared to previous reports in order to improve charge injection from the PbS into the ZnO electrode and increase the V_{OC}.[2,11,42]

We systematically optimized the thickness of both I$_2$-treated and non-I$_2$-treated CQD devices (Figure S4, Supporting Information). By using the I$_2$-treated CQDs throughout the entire thickness of the active layer of the best devices, we were able to increase the device thickness by one extra CQD layer without losing the fill factor (Figure 2b,c), which is an indication of improved passivation that yields longer carrier diffusion length.

External quantum efficiency (EQE) spectra shown in Figure 2d confirm that the extra photocarriers generated in a thicker device can still be successfully extracted (double-pass absorption of the devices can be seen in Figure S5 in the Supporting Information). Current–voltage characteristics of the representative devices under simulated AM1.5G illumination are shown in Figure 2e, with the relevant figures of merit and statistical analysis summarized in **Table 1**. For I$_2$-treated devices, a PCE of 10.2% was measured in our lab with a certified PCE of 9.9% (Figure S6, Supporting Information), were achieved for I$_2$-treated dots. The 10.2% is significantly higher than the PCE of 9.2% obtained for non-I$_2$-treated control samples (see Table 1). The extra PCE point is the result of improved J_{sc} and fill factor (FF).

In order to gain insight into the physical origins of the improved performance, we built an optoelectronic device model (**Figure 3**a) that takes into account the electron affinity of CQDs with different ligand treatments, absorption profiles, thicknesses, and carrier diffusion lengths starting from previously reported values for TBAI-treated films.[11,25,43] The improvement of the EQE in the longer wavelength region can be fully attributed to the increased device thickness (Figure 3c). However, for a constant photocarrier diffusion length, the increased device thickness can eventually result in a deterioration of the charge collection. Holes photoexcited near the front electrode have the longest distance to travel and therefore experience this limitation first, resulting in an EQE drop in the blue region. Therefore, the improvement in the EQE over all wavelengths observed experimentally for I$_2$-treated dots can only be justified by both a thicker active region and a longer effective diffusion length, given that the mobility has not been affected (Figure S7, Supporting Information). Figure 3b,c shows this phenomenon for the case when the diffusion length is chosen to differ by ≈50% (to visually amplify the difference in EQE). Experimentally observed differences are more subtle. The increase in fill factor and short-circuit current density can be reproduced with 80 nm and 110 nm carrier diffusion lengths for control and I$_2$-treated films, respectively (see Figure S8, Supporting Information). Such an increase in diffusion length allows for thicker devices while maintaining efficient carrier collection, leading to a full power point improvement in device performance.

To further validate the predictions of the theoretical model, we measured experimentally the carrier collection efficiency (η)
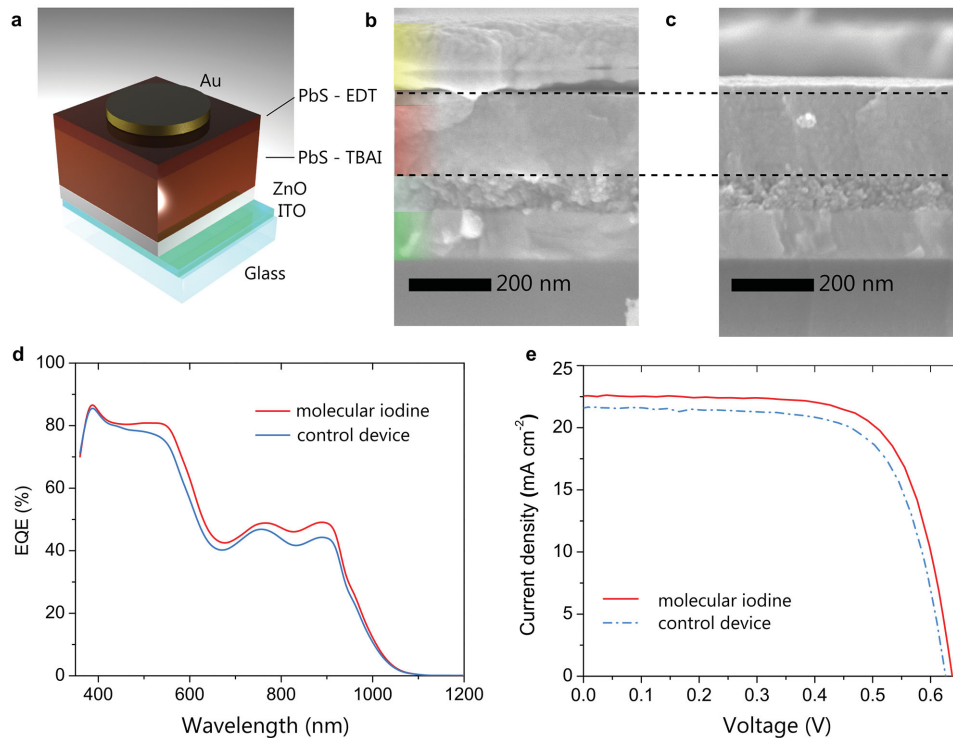
Figure 2. Device architecture and performance. a) Schematic of the device structure. A TBAI-exchanged CQD film is deposited on top of a ZnO electrode, followed by two layers of EDT-exchanged CQDs and gold as the top contact. b,c) Cross-sectional SEM images of a 200 nm CQD thick control device and a 220 nm thick I$_2$ treated PbS CQD device (also see note in Section S10 of the Supporting Information). d) EQE of the control and I$_2$-treated CQD devices. Fabry–Perot effects visibly change the shape of the EQE compared to single-pass absorption spectra. e) J–V characteristics under simulated AM1.5G illumination for the control and I$_2$-treated devices. A PCE = 10.18% is obtained for molecular-iodine treated dots as a result of increased J_{sc} and FF.

of the I$_2$-treated and control devices (**Figure 4**a). We used an analytical model also employed in prior reports to fit the experimental data.[44]

$$\eta(V) = \text{IQE}(\lambda) \frac{J_H(V) - J_L(V)}{J_{sc,H} - J_{sc,L}} \qquad (1)$$

where IQE(λ) is the internal quantum efficiency at short-circuit condition under monochromatic illumination (λ = 820 nm), and J_H and J_L are the currents at two different powers for the same illumination (see the Experimental Section for more details). By fitting η one can estimate the diffusion length of the CQD films. The experiment confirms that the molecular iodine treatment increases diffusion length substantially, from 85 to 115 nm, which is in a good agreement with the diffusion lengths obtained from optoelectronic device simulations.

Given the similar depletion widths of the control and I$_2$ treated devices (≈85 nm at maximum power point, Figure S9, Supporting Information), we can pinpoint diffusion length to be responsible for the improved J_{sc} and FF.

Since the carrier diffusion length is primarily determined by the electronic trap state density in the CQD solid, we sought to verify how the trap density is affected by molecular iodine treatment by using transient photovoltage measurements.[27] Based on the photovoltage studies, we observed a two-fold reduction in the trap density for I$_2$-treated dots at the maximum power point condition (Figure 4b). From $L_D = \sqrt{D\tau}$, where the lifetime τ is inversely proportional to the trap density,[45,46] this predicts a factor of improvement of ≈√2 (i.e., ≈40% increase) in the diffusion length, which is in a good agreement with the 35% increase obtained experimentally. The reduced trap density is also in agreement with the increase of V_{OC} in I$_2$-treated devices.

In conclusion, we have demonstrated that molecular iodine improves the passivation of traps in PbS CQDs. We find that these remnant traps are not addressed using prior solid-state ligand exchange treatments. A twofold decrease in trap density in the molecular iodine-treated CQD film leads to improved diffusion length and a full power point increase in device performance. This improvement resulted in a certified PCE of 9.9%, a new record for colloidal quantum dot solar cells.

Table 1. Static figures of merit for the control and I$_2$-treated devices. Statistics is based on 49 different devices.
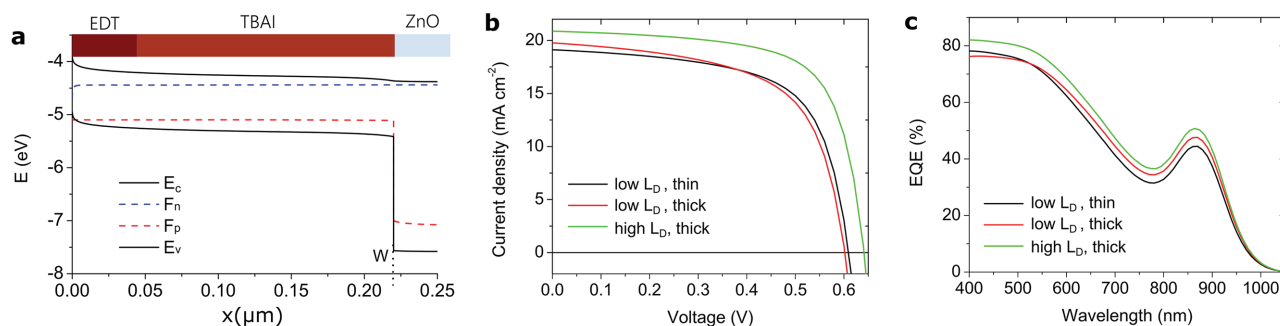
	V_{oc} [V]	J_{sc} [mA cm^{-2}]	FF[a] [%]	PCE[b] [%]
Control devices	0.632 ± 0.004	21.40 ± 0.31	69.47 ± 0.98	9.24 ± 0.13
Molecular iodine devices	0.639 ± 0.004	22.28 ± 0.27	72.37 ± 0.94	10.18 ± 0.20

[a]Fill factor (FF); [b]Power conversion efficiency (PCE).

Figure 3. Optoelectronic model of the origin of improved device performance. a) Band diagram of the graded device at open-circuit voltage conditions. E_c, F_n, F_p, and E_v describe, respectively, the energy level of the conduction band, quasi-Fermi level of electrons and holes, and valence band across the length of the device (x). b) J–V curves and c) simulated EQEs demonstrating the effect of the device thickness and carrier diffusion length, L_D, on the device performance and EQE, respectively.
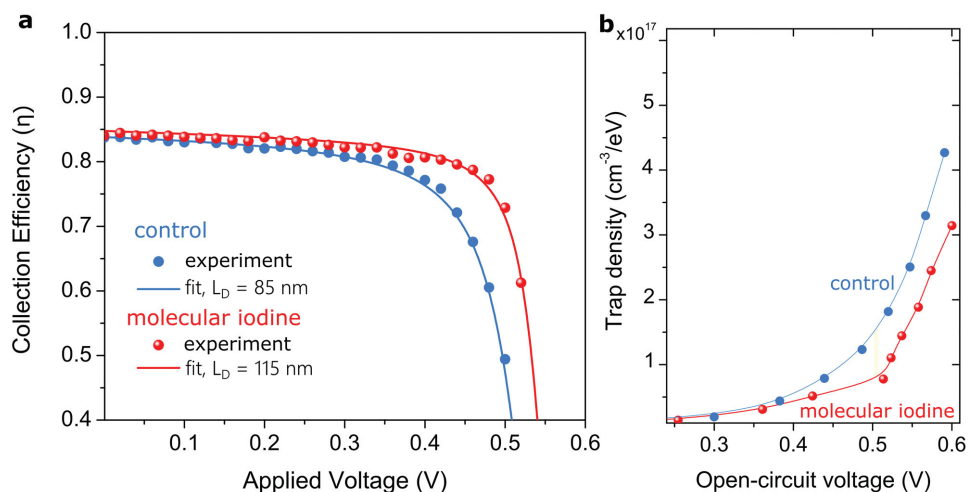
Experimental Section

CQD Synthesis and I_2 Treatment of PbS QDs: PbS QDs were prepared following previous reports.[11,27] When the reaction flask was cooled to 30–35 °C, the nanoparticles were separated from the growth solution by adding 60 mL of acetone followed by centrifugation. The isolated nanoparticles were then dried in vacuum for 12 h and redispersed in toluene (150 mg mL^{-1}) and transferred to a nitrogen glovebox. For the solution I_2 treatment, 0.5 mL I_2-toluene (25×10^{-3} M) solution was added, in a drop-by-drop fashion, to the PbS nanocrystal solution (2.5 mL) in a vial. The solution was kept in the glovebox for 24 h. Methanol was employed to precipitate the nanocrystals. Following fully drying, the nanocrystals were finally dispersed in octane (50 mg mL^{-1}). The purified untreated PbS QDs (50 mg mL^{-1}) were achieved by using similar procedures.

ZnO Nanoparticle Synthesis and Film Deposition: The synthesis of ZnO nanoparticles is similar to methods reported previously.[2] After the reaction, the nanoparticles were separated from the solution by centrifugation, followed by a two-time purification process by methanol. The nanoparticles were finally dispersed in a mixture of chloroform and methanol. For the preparation of ZnO electrode, the ZnO nanocrystal solution was spin-cast on ITO glass at 6000 rpm for 10 s.

Material Characterization: Scanning electron microscopy (SEM) and transmission electron microscopy (TEM) characterization were obtained on a Hitachi S-5200 scanning electron microscope. Optical absorption measurements were carried out in a Lambda 950 500 UV–vis–IR spectrophotometer. Photoluminescence measurements were carried out using a 442 nm blue laser and an Ocean Optics NIR-512 spectrophotometer. Absolute PLQY measurements were done using a Horiba Fluorolog Time Correlated Single Photon Counting system equipped with UV/vis/NIR photomultiplier tube detectors, dual grating spectrometers, and a monochromatized xenon lamp excitation source. An accompanying Quanta-Phi integrating sphere with an excitation wavelength of 635 nm was employed. Quantum dots were dispersed in toluene in quartz cuvettes. The quantum-dot concentration was kept constant between samples by measuring the absorbance spectra and adjusting the samples accordingly.

XPS measurements were performed using a Thermo Scientific K-Alpha system with electron-gun compensation to avoid sample charging and with 50 eV pass energy and binding energy step of 0.03–0.05 eV. All intensities were normalized to the Pb signal, and all binding energies were calibrated by setting the C 1s signal to 285 eV.

Device Fabrication: PbS QDs were deposited using a layer-by-layer spin-casting process. A 6 mL syringe capped with a 0.22 μm filter was

Figure 4. Experimental determination of diffusion length and improved passivation. a) Collection efficiency and diffusion length for control and molecular I_2-treated dots. A 35% increase is observed for I_2 treated devices, b) density of trap states extracted from V_{OC} decay measurements for control and I_2-treated films. The better passivation of molecular iodine leads to a twofold reduction in the trap density at maximum power point conditions, which is in agreement with the observed increase in the diffusion length.

used for the deposition of PbS QDs. The volume for each layer was 2 drops, ≈50 µL. For the TBAI layer, two drops of PbS CQDs in octane (50 mg mL^{-1}) were deposited onto the ZnO substrates and were spin-cast at 2500 rpm for 10 s. The film was soaked in TBAI (10 mg mL^{-1}) containing methanol solution and spun after 30 s at the same speed for 10 s. This was followed by a two-time methanol rinse process. The process was repeated 7–8 times, for the control and the I$_2$ devices, respectively. Following the TBAI stack of layers, two layers of EDT-exchanged PbS QDs were deposited for both cases. In a typical process, PbS was deposited with the same procedure as applied for the TBAI layers. A 0.01% v:v EDT:acetonitrile solution was deposited on the film and spun after soaking for 30 s, which was followed by a three-time acetonitrile rinsing process. For the top electrode, 120 nm Au was deposited on the PbS film to complete the device.

Device Characterization: J–V Characterization: Current–voltage traces were acquired with a Keithley 2400 source measuring unit under simulated AM1.5G illumination (Sciencetech class A). The spectral mismatch was calibrated using a reference solar cell (Newport), yielding a correction multiplicative factor of $M = 0.848$. Devices were measured under a continuous flow of nitrogen gas. In the performance measurements, we used a copper aperture to define the device area to be ≈0.049 cm^2.

EQE Measurement: External-quantum-efficiency spectra were taken by subjecting the cells to monochromatic illumination (400 W Xe lamp passing through a monochromator and appropriate cut-off filters). The output power was calibrated with Newport 818-UV and Newport 838-IR photodetectors. The beam was chopped at 220 Hz and focused in the pixel together with a solar-simulator at 1 sun intensity to provide for light bias. The response of the cell was acquired with a Lakeshore preamplifier connected to Stanford Research 830 lock-in amplifier at short-circuit conditions.

Capacitance–Voltage Measurement: The capacitance–voltage measurements were acquired with an Agilent 4284A LCR meter at a frequency of 1 kHz and an AC signal of 50 mV, scanning from −1 to 1 V. From the capacitance measurement (C) the depletion width (L_{dep}) can be calculated as:

$$L_{dep} = \frac{\varepsilon A}{C} \qquad (2)$$

where A is the area of the device and ε is the static permittivity of the PbS CQD solid (see Section S9 of the Supporting Information for further details).

Trap-Spectroscopy Measurements: The trap density of the films in the final device architecture was obtained by combining current and voltage transient spectroscopy at different open-circuit voltages as previously reported.[27] Various V_{oc} were achieved by 640 nm by a light-bias laser light passing through different filters. A small signal perturbation (ca. 10 mV) was generated with a 640 nm Melles-Griot laser modulated with an Agilent 33220A waveform generator (50 Hz period, 5 µs pulse). Short-circuit and open-circuit conditions were established by selecting the input impedance of the recording oscilloscope (Tektronix TDS 5104).

Diffusion Length Measurement: The diffusion length of the devices was measured based on a previously introduced model.[44] The collection efficiency (η) can be calculated as follows:

$$\eta(V) = IQE(\lambda_i, V = 0) \frac{J_H(V, \lambda_i) - J_L(V, \lambda_i)}{J_H(V = 0, \lambda_i) - J_L(V = 0, \lambda_i)} \qquad (3)$$

where H and L subscripts stand for higher and lower power J–V curves under $\lambda = 820$ nm monochromatic illumination ($L = 4$ µW and $H = 20$ µW). The IQE is taken at the excitation wavelength at short-circuit ($V = 0$) conditions from the EQE and the absorption at this wavelength. The diffusion length can be estimated by fitting the experimental data to this analytical model. The employed thicknesses correspond to those of the photovoltaic devices under study (200 nm and 220 nm of CQD film for the control and the I$_2$-treated samples, respectively).

Optoelectronic Simulations: Optoelectronic simulations were performed using SCAPS software.[47] The complete set of simulation parameters is included in Section S11 of the Supporting Information.

Supporting Information

Supporting Information is available from the Wiley Online Library or from the author.

Acknowledgements

[1] S. A. Mcdonald, G. Konstantatos, S. Zhang, P. W. Cyr, E. J. Klem, L. Levina, E. H. Sargent, *Nat. Mater.* **2005**, *4*, 138.

[2] C.-H. M. Chuang, P. R. Brown, V. Bulović, M. G. Bawendi, *Nat. Mater.* **2014**, *13*, 796.

[3] A. J. Labelle, S. M. Thon, S. Masala, M. M. Adachi, H. Dong, M. Farahani, A. H. Ip, A. Fratalocchi, E. H. Sargent, *Nano Lett.* **2015**, *15*, 1101.

[4] G. H. Carey, L. Levina, R. Comin, O. Voznyy, E. H. Sargent, *Adv. Mater.* **2015**, *27*, 3325.

[5] A. H. Ip, A. Kiani, I. J. Kramer, O. Voznyy, H. F. Movahed, L. Levina, M. M. Adachi, S. Hoogland, E. H. Sargent, *ACS Nano* **2015**, *9*, 8833.

[6] M. M. Lee, J. Teuscher, T. Miyasaka, T. N. Murakami, H. J. Snaith, *Science* **2012**, *338*, 643.

[7] S. R. Wenham, M. A. Green, *Prog. Photovoltaics: Res. Appl.* **1996**, *4*, 3.

[8] A. G. Midgett, J. M. Luther, J. T. Stewart, D. K. Smith, L. A. Padilha, V. I. Klimov, A. J. Nozik, M. C. Beard, *Nano Lett.* **2013**, *13*, 3078.

[9] O. E. Semonin, J. M. Luther, S. Choi, H.-Y. Chen, J. Gao, A. J. Nozik, M. C. Beard, *Science* **2011**, *334*, 1530.

[10] J. M. Luther, J. Gao, M. T. Lloyd, O. E. Semonin, M. C. Beard, A. J. Nozik, *Adv. Mater.* **2010**, *22*, 3704.

[11] Z. Ning, O. Voznyy, J. Pan, S. Hoogland, V. Adinolfi, J. Xu, M. Li, A. R. Kirmani, J.-P. Sun, J. Minor, K. W. Kemp, H. Dong, L. Rollny, A. Labelle, G. Carey, B. Sutherland, I. Hill, A. Amassian, H. Liu, J. Tang, O. M. Bakr, E. H. Sargent, *Nat. Mater.* **2014**, *13*, 822.

[12] X. Wang, G. I. Koleilat, J. Tang, H. Liu, I. J. Kramer, R. Debnath, L. Brzozowski, D. A. R. Barkhouse, L. Levina, S. Hoogland, E. H. Sargent, *Nat. Photonics* **2011**, *5*, 480.

[13] X. Lan, S. Masala, E. H. Sargent, *Nat. Mater.* **2014**, *13*, 233.

[14] D. Paz-Soldan, A. Lee, S. M. Thon, M. M. Adachi, H. Dong, P. Maraghechi, M. Yuan, A. J. Labelle, S. Hoogland, K. Liu, E. Kumacheva, E. H. Sargent, *Nano Lett.* **2013**, *13*, 1502.

[15] T. Kawawaki, H. Wang, T. Kubo, K. Saito, J. Nakazaki, H. Segawa, T. Tatsuma, *ACS Nano* **2015**, *9*, 4165.

[16] A. Mihi, F. J. Beck, T. Lasanta, A. K. Rath, G. Konstantatos, *Adv. Mater.* **2014**, *26*, 443.

[17] K. W. Johnston, A. G. Pattantyus-Abraham, J. P. Clifford, S. H. Myrskog, S. Hoogland, H. Shukla, E. J. Klem, L. Levina, E. H. Sargent, *Appl. Phys. Lett.* **2008**, *92*, 122111.

[18] A. G. Pattantyus-Abraham, I. J. Kramer, A. R. Barkhouse, X. Wang, G. Konstantatos, R. Debnath, L. Levina, I. Raabe,

M. K. Nazeeruddin, M. Grätzel, E. H. Sargent, *ACS Nano* **2010**, *4*, 3374.

[19] J. M. Luther, M. Law, M. C. Beard, Q. Song, M. O. Reese, R. J. Ellingson, A. J. Nozik, *Nano Lett.* **2008**, *8*, 3488.

[20] X. Lan, J. Bai, S. Masala, S. M. Thon, Y. Ren, I. J. Kramer, S. Hoogland, A. Simchi, G. I. Koleilat, D. Paz-Soldan, Z. Ning, A. J. Labelle, J. Y. Kim, G. Jabbour, E. H. Sargent, *Adv. Mater.* **2013**, *25*, 1769.

[21] J. Jean, S. Chang, P. R. Brown, J. J. Cheng, P. H. Rekemeyer, M. G. Bawendi, S. Gradecak, V. Bulovic, *Adv. Mater.* **2013**, *25*, 2790.

[22] H. Wang, T. Kubo, J. Nakazaki, T. Kinoshita, H. Segawa, *J. Phys. Chem. Lett.* **2013**, *4*, 2455.

[23] A. K. Rath, M. Bernechea, L. Martinez, F. P. G. de Arquer, J. Osmond, G. Konstantatos, *Nat. Photonics* **2012**, *6*, 529.

[24] B. A. Gonfa, M. R. Kim, N. Delegan, A. C. Tavares, R. Izquierdo, N. Wu, M. A. El Khakani, D. Ma, *Nanoscale* **2015**, *7*, 10039.

[25] Z. Ning, D. Zhitomirsky, V. Adinolfi, B. Sutherland, J. Xu, O. Voznyy, P. Maraghechi, X. Lan, S. Hoogland, Y. Ren, *Adv. Mater.* **2013**, *25*, 1719.

[26] J. Tang, H. Liu, D. Zhitomirsky, S. Hoogland, X. Wang, M. Furukawa, L. Levina, E. H. Sargent, *Nano Lett.* **2012**, *12*, 4889.

[27] A. H. Ip, S. M. Thon, S. Hoogland, O. Voznyy, D. Zhitomirsky, R. Debnath, L. Levina, L. R. Rollny, G. H. Carey, A. Fischer, K. W. Kemp, I. J. Kramer, Z. Ning, A. J. Labelle, K. W. Chou, A. Amassian, E. H. Sargent, *Nat. Nanotechnol.* **2012**, *7*, 577.

[28] J. M. Luther, J. M. Pietryga, *ACS Nano* **2013**, *7*, 1845.

[29] S. J. Oh, N. E. Berry, J.-H. Choi, E. A. Gaulding, T. Paik, S.-H. Hong, C. B. Murray, C. R. Kagan, *ACS Nano* **2013**, *7*, 2413.

[30] O. Voznyy, D. Zhitomirsky, P. Stadler, Z. Ning, S. Hoogland, E. H. Sargent, *ACS Nano* **2012**, *6*, 8448.

[31] J. H. Engel, A. P. Alivisatos, *Chem. Mater.* **2014**, *26*, 153.

[32] S. M. Thon, A. H. Ip, O. Voznyy, L. Levina, K. W. Kemp, G. H. Carey, S. Masala, E. H. Sargent, *ACS Nano* **2013**, *7*, 7680.

[33] J. Tang, K. W. Kemp, S. Hoogland, K. S. Jeong, H. Liu, L. Levina, M. Furukawa, X. Wang, R. Debnath, D. Cha, *Nat. Mater.* **2011**, *10*, 765.

[34] D. K. Ko, P. R. Brown, M. G. Bawendi, V. Bulović, *Adv. Mater.* **2014**, *26*, 4845.

[35] J.-H. Choi, A. T. Fafarman, S. J. Oh, D.-K. Ko, D. K. Kim, B. T. Diroll, S. Muramoto, J. G. Gillen, C. B. Murray, C. R. Kagan, *Nano Lett.* **2012**, *12*, 2631.

[36] M. Ibáñez, R. J. Korkosz, Z. Luo, P. Riba, D. Cadavid, S. Ortega, A. Cabot, M. G. Kanatzidis, *J. Am. Chem. Soc.* **2015**, *137*, 4046.

[37] J. Tang, E. H. Sargent, *Adv. Mater.* **2011**, *23*, 12.

[38] F. Jähnig, D. Bozyigit, O. Yarema, V. Wood, *APL Mater.* **2015**, *3*, 020701.

[39] W. K. Bae, J. Joo, L. A. Padilha, J. Won, D. C. Lee, Q. Lin, W.-k. Koh, H. Luo, V. I. Klimov, J. M. Pietryga, *J. Am. Chem. Soc.* **2012**, *134*, 20160.

[40] D. Zhitomirsky, M. Furukawa, J. Tang, P. Stadler, S. Hoogland, O. Voznyy, H. Liu, E. H. Sargent, *Adv. Mater.* **2012**, *24*, 6181.

[41] O. Voznyy, S. Thon, A. Ip, E. Sargent, *J. Phys. Chem. Lett.* **2013**, *4*, 987.

[42] C.-H. M. Chuang, A. Maurano, R. E. Brandt, G. W. Hwang, J. Jean, T. Buonassisi, V. Bulović, M. G. Bawendi, *Nano Lett.* **2015**, *15*, 3286.

[43] P. R. Brown, D. Kim, R. R. Lunt, N. Zhao, M. G. Bawendi, J. C. Grossman, V. Bulović, *ACS Nano* **2014**, *8*, 5863.

[44] K. Kemp, C. Wong, S. Hoogland, E. Sargent, *Appl. Phys. Lett.* **2013**, *103*, 211101.

[45] D. Zhitomirsky, O. Voznyy, L. Levina, S. Hoogland, K. W. Kemp, A. H. Ip, S. M. Thon, E. H. Sargent, *Nat. Commun.* **2014**, *5*, 3803.

[46] D. Zhitomirsky, O. Voznyy, S. Hoogland, E. H. Sargent, *ACS Nano* **2013**, *7*, 5282.

[47] M. Burgelman, K. Decock, S. Khelifi, A. Abass, *Thin Solid Films* **2013**, *535*, 296.